Hindawi Publishing Corporation
Journal of Construction Engineering
Volume 2013, Article ID 874180, 10 pages
http://dx.doi.org/10.1155/2013/874180

Research Article

Seismic Analysis of Deep Water Pile Foundation Based on Three-Dimensional Potential-Based Fluid Elements

Kai Wei and Wancheng Yuan

State Key Laboratory of Disaster Reduction in Civil Engineering, Tongji University, Shanghai 200092, China

Correspondence should be addressed to Kai Wei; kaiwei.tj@gmail.com

Received 28 December 2012; Accepted 8 March 2013

Academic Editor: Eric Lui

This paper investigates the use of three-dimensional (3D) $\phi - u$ potential-based fluid elements for seismic analyses of deep water pile foundation. The mathematical derivations of the potential-based formulations are presented for reference. The potential-based modeling technique is studied and validated through experimental data and analytical solutions. Earthquake time history analyses for a 9-pile foundation in dry and different water environments are conducted, respectively. The seismic responses are discussed to investigate the complex effect of earthquake-induced fluid-structure interaction. Through the analyses, the potential-based fluid and interface elements are shown to perform adequately for the seismic analyses of pile foundation-water systems, and some interesting conclusions and recommendations are drawn.

1. Introduction

Bridges are popular solutions for crossing gaps caused by rivers, reservoirs, straits, or bays. These bridges usually have long spans and need to be supported by deep water foundations [1]. One of the common choices is using deep water pile foundations due to their low cost and ease of construction [2, 3]. This type of foundation consists of piles, a concrete cap, and piers or towers, where piles and pile cap are usually immersed in the water [4, 5]. Previous research [6–8] showed that the interaction between the structure and the surrounding water might alter the dynamic characteristics, which may lead to additional dynamic forces.

The earliest approaches to account for the hydrodynamic force on the cylindrical objects were drawn from experimental data and presented in terms of "added mass" [9]. Although it lacked theoretical derivation, "added mass" is still a widely used concept because of its simplicity [10–12]. The analytical dynamics of cantilever towers in water was then developed mathematically, including structural flexibility and water compressibility effects [13]. Many later investigations followed it and continued to study the fluid-structure interactions of the single immersed cylinder [14, 15]. Although the single pile problem has been studied thoroughly, the pile-group-water interaction is still hard to solve due to the mathematical difficulties in modelling the complex interfaces and boundaries.

Rapid development of computer techniques motivated scientists to find numerical methods to overcome those analytical limitations. Numerous approaches based on either finite elements or boundary elements were proposed in the last few years [16, 17]. Potential-based fluid element (PBFE) was proposed in 1980s [18]. Today it has been successfully applied to fluid-structure frequency- and time-domain dynamic analysis of dam-reservoir interaction problem and has beenverified by experimental and analytical results [19, 20]. However, little attention has been paid to the three-dimensional (3D) modeling for seismic analysis of deep water pile foundation using PBFE. The review of current work by many researchers indicated that it was hard to carry out seismic analysis of deep water bridge structures. Therefore, the objective of this paper is to investigate the

performance of the 3D PBFEs for the seismic analyses of pile foundation-water systems and to present an alternative finite element approach for future research. The complex effects of the earthquake-induced fluid-structure interaction are investigated through time-domain seismic analyses of a common pile foundation-water system.

2. Theory of Potential-Based Fluid Elements

The formulations of PBFE and interface elements adopted in this study are firstly reviewed in this section.

2.1. Formulation of the $\phi - u$ Potential-Based Fluid Elements. In formulation of potential-based fluid elements, two unknown variables of fluid particle are fluid potential ϕ and displacement u. To derive the governing differential equations for the fluid, the usual acoustic wave theory approximations are made as follows [21].

(i) The fluid motion is assumed to be inviscid, slightly compressible, and adiabatic:

$$\frac{\rho}{\rho_w} = 1 + \frac{p}{\mu}. \tag{1}$$

(ii) Body forces are neglected:

$$\Omega(x) = 0. \tag{2}$$

(iii) Fluid velocity and density changes are infinitesimally small:

$$\nabla\phi \approx 0, \qquad \rho \approx \rho_w, \qquad h = \int \frac{dp}{\rho} \approx \frac{p}{\rho_w}, \tag{3}$$

in which ρ is the density of water, ρ_w is the nominal density of water, p is the hydrodynamic pressure, $\mu = \rho C^2$ is the bulk modulus of water, C is the sound velocity in water with a value of 1440 m/s, $\Omega(x)$ is the potential of the body force accelerations at position x, ∇ is the vector gradient, and h is the specific enthalpy of the fluid particle. With these assumptions, the velocity potential ϕ satisfies [22] the following.

(1) The continuity equation:

$$\frac{\partial\rho}{\partial t} + \nabla(\rho\nabla\phi) \approx \frac{\partial\rho}{\partial t} + \rho_w\nabla^2\phi \approx \frac{\rho_w}{\mu}\frac{\partial p}{\partial t} + \rho_w\nabla^2\phi = 0, \tag{4}$$

where t is the time variable, from which, we see

$$\nabla^2\phi = -\frac{1}{\mu}\frac{\partial p}{\partial t}. \tag{5}$$

(2) The momentum/equilibrium equation for the fluid:

$$h = \Omega(x) - \frac{\partial\phi}{\partial t} - \frac{1}{2}\nabla\phi\nabla\phi \approx -\frac{\partial\phi}{\partial t}. \tag{6}$$

Substituting (3) and (6) into (5) gives the special form of the Helmholtz wave equation:

$$\nabla^2\phi = -\frac{\rho_w}{\mu}\frac{\partial h}{\partial t} = \frac{1}{C^2}\frac{\partial^2\phi}{\partial t^2}. \tag{7}$$

To establish a virtual work expression, we consider a weak form of (7):

$$\int_{V_r} \nabla^2\phi\delta\phi \, dV = \int_{V_r} \frac{1}{C^2}\frac{\partial^2\phi}{\partial t^2}\delta\phi \, dV, \tag{8}$$

where the right-hand side is the standard d'Alembert force integral and the left-hand side can be integrated using the vector identity $\nabla^2\phi\delta\phi = \nabla(\nabla\phi\delta\phi) - \nabla\phi\nabla(\delta\phi)$. Then we obtain

$$\int_{V_r} \nabla(\nabla\phi\cdot\delta\phi)\, dV - \int_{V_r} \nabla\phi\cdot\nabla(\delta\phi)\, dV = \int_{V_r} \frac{1}{C^2}\frac{\partial^2\phi}{\partial t^2}\delta\phi \, dV. \tag{9}$$

According to the divergence theorems, the first term of the left-hand side can be rewritten as

$$\int_{V_r} \nabla(\nabla\phi\cdot\delta\phi)\, dV = -\int_{S_r} \frac{\partial u}{\partial t}\mathbf{n}\delta\phi \, dS. \tag{10}$$

Hence, we obtain the variational form of (7) in the fluid potential ϕ

$$\begin{aligned}\frac{\rho}{C^2}\int_{V_r}\frac{\partial^2\phi}{\partial t^2}\delta\phi \, dV + \rho\int_{S_r}\frac{\partial u}{\partial t}\mathbf{n}\delta\phi \, dS \\ + \rho\int_{V_r}\nabla\phi\cdot\nabla\delta\phi \, dV = 0,\end{aligned} \tag{11}$$

where V_r indicates the volume of pile, S_r is a water boundary where normal velocity is prescribed, and $\mathbf{n}$ is unit normal on S_r pointing into the fluid. Under an earthquake excitation, the dynamic response of the pile and the water is coupled through compatibility of velocity potential and prescribed normal velocity at the pile-water interface. The finite element system matrices corresponding to the coupled pile foundation-water system are

$$\begin{aligned}&\begin{bmatrix} M_{ss} & 0 \\ 0 & -M_{rr}\end{bmatrix}\begin{bmatrix}\ddot{U}\\ \ddot{\Phi}\end{bmatrix} + \begin{bmatrix} C_{ss} & C_{sr} \\ C_{rs} & 0\end{bmatrix}\begin{bmatrix}\dot{U}\\ \dot{\Phi}\end{bmatrix} + \begin{bmatrix} K_{ss} & 0 \\ 0 & -K_{rr}\end{bmatrix}\begin{bmatrix}U\\ \Phi\end{bmatrix} \\ &= \begin{bmatrix} -M_{ss}\mathbf{l}\ddot{u}_g(t) \\ -C_{rs}\mathbf{l}\dot{u}_g(t)\end{bmatrix},\end{aligned} \tag{12}$$

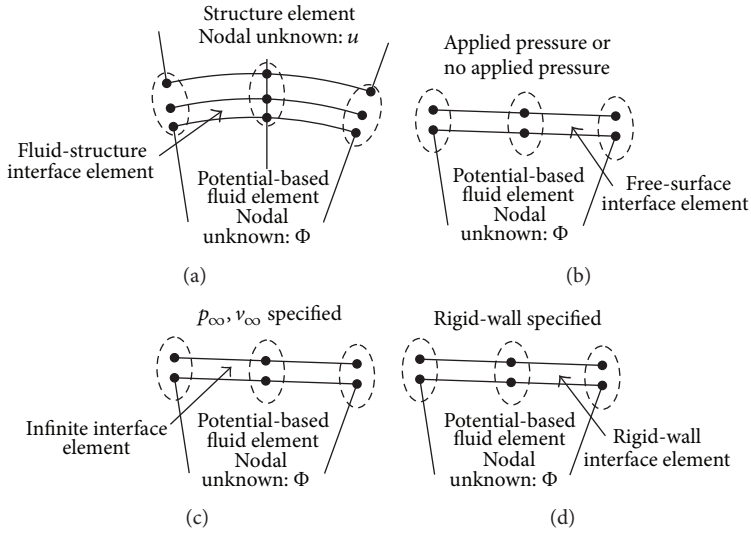

Figure 1: Interface elements used in PBFE modeling.

with

$$M_{ss} = \rho_s \int_{V_s} \psi_s^T \psi_s dV, \qquad M_{rr} = \frac{\rho}{C^2} \int_{V_r} \psi_r^T \psi_r dV,$$

$$K_{ss} = \rho_s \int_{V_s} \psi_s^T D_s^T \psi_s dV,$$

$$K_{rr} = \rho \int_{V_r} B_r^T B_r dV, \qquad C_{sr} = -\rho \int_{s_r} \psi_s^T n \psi_s dS,$$

$$C_{rs} = C_{sr}^T,$$

$$C_{ss} = a_R M_{ss} + b_R K_{ss}, \qquad B_r = \begin{bmatrix} \frac{\partial \psi_r^{(1)}}{\partial x} & \frac{\partial \psi_r^{(2)}}{\partial x} & \cdots & \frac{\partial \psi_r^{(n_r)}}{\partial x} \\ \frac{\partial \psi_r^{(1)}}{\partial y} & \frac{\partial \psi_r^{(2)}}{\partial y} & \cdots & \frac{\partial \psi_r^{(n_r)}}{\partial y} \end{bmatrix}, \tag{13}$$

where U and Φ are the nodal displacement vector and the nodal velocity potential vector, respectively; ψ_s and ψ_r are the standard isoparametric shape function matrices for 3D solid and fluid elements, respectively; ρ_s and V_s are the mass density and volume of the foundation concrete, respectively; D_s is the elasticity matrix of solid elements; n_r denotes the number of nodes per fluid element. Column vector $\mathbf{1}$ has the same dimension and order as the vector of nodal relative displacements U. It contains ones when a translational degree of freedom corresponds to the direction of earthquake excitation and zeros otherwise. Earthquake loading $\ddot{u}_g(t)$ can be applied as a mass-proportional body force. Submatrices M_{ss} and K_{ss} represent the mass and stiffness matrices for the structural substructures, and M_{rr} and K_{rr} represent those for the water. Submatrices C_{rs} and C_{sr} account for pile foundation-water interaction through enforced equilibrium and compatibility at fluid-structure interface. Coefficients a_R and b_R are used to define a Rayleigh damping matrix C_{ss} for the foundation substructure. Using Fourier transform of the left-hand side, the jth eigenvalue equation of the coupled system can be derived from (12):

$$\left(-\omega_j^2 \begin{bmatrix} M_{ss} & 0 \\ 0 & M_{rr} \end{bmatrix} - \omega_j \begin{bmatrix} 0 & C_{sr} \\ C_{rs} & 0 \end{bmatrix} + \begin{bmatrix} K_{ss} & 0 \\ 0 & K_{rr} \end{bmatrix}\right) \times \begin{bmatrix} U^{(j)} \\ F^{(j)} \end{bmatrix} = \begin{bmatrix} 0 \\ 0 \end{bmatrix}, \tag{14}$$

where $F^{(j)} = -i\Phi^{(j)}$, $i = \sqrt{-1}$. Equations (12) and (14) show that time-domain and frequency-domain analyses are all feasible in the 3D numerical model with solid and potential-based fluid elements. It will be very useful for seismic analyses of deep water bridge foundation.

2.2. Interface Elements. Interface elements are required on the bounding surface of the fluid domain to construct the model. Hereby, we introduce four boundary conditions for ϕ–u potential-based interface elements, which are commonly used for seismic analysis:

(i) at the fluid-structure interface (Figure 1(a)):

$$\frac{\partial \phi}{\partial \mathbf{n}} = \frac{\partial u}{\partial t}\mathbf{n}, \tag{15}$$

(ii) at the free surface interface (Figure 1(b)):

$$\phi = 0, \tag{16}$$

(iii) at the infinite interface (Figure 1(c)):

$$\frac{\partial \phi}{\partial t} = p_\infty, \qquad \frac{\partial \phi}{\partial \mathbf{n}} = \frac{\partial u_\infty}{\partial t}\mathbf{n}, \tag{17}$$

(iv) at the rigid-wall interface (Figure 1(d)):

$$\phi = 0, \qquad \frac{\partial \phi}{\partial \mathbf{n}} = 0, \tag{18}$$

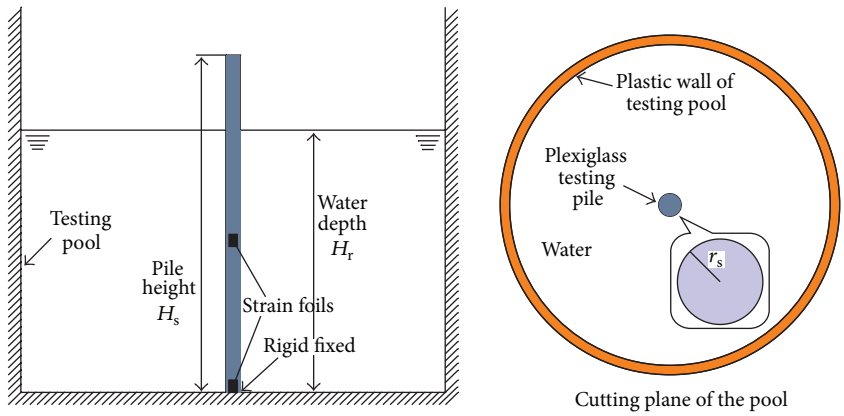

Figure 2: Setup of the pile-water system experiment.

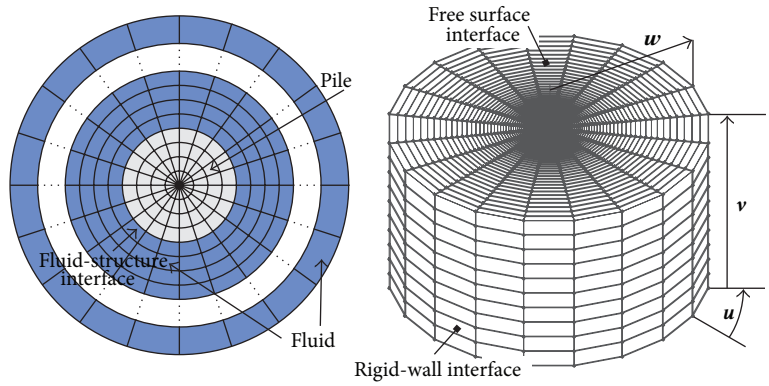

Figure 3: PBFE model.

where **n** is the unit vector normal to the pile surface, $U_{\mathbf{n}}$ is the corresponding normal displacement, and $\partial u_\infty/\partial t$ and p_∞ are the corresponding normal velocity and pressure at infinity, respectively.

3. Validation of 3D PBFE Approach

3.1. Experiment Description. Zhang [23] had carried out a frequency experiment for the single pile-water system as shown in Figure 2. The Plexiglas cantilever pile model had a radius r_s of 0.0146 m, a height H_s of 0.55 m, a Young's modulus E_s of 2.44×10^3 MPa, and a unit mass μ_s of 0.696 Kg/m. The surrounding water was filled in a cylinder basin with a diameter of 1 m, a depth of 0.63 m, a density ρ_w of 1000 Kg/m^3, and a bulk modulus of 2.30×10^3 MPa. The fundamental natural frequency of the system at four water levels of 0 m, 0.44 m, 0.52 m, and 0.55 m was tested, respectively.

3.2. Finite Element Modeling. High-density division and refined element mesh will not only give us accurate results but also burden us with poor computing efficiency. It is a common practice that the largest mesh size along **v** and the size ratio of the adjacent solid and fluid element l_f/l_s along **w** axis influence the accuracy of the fluid-structure interaction significantly, in which **u**, **v**, and **w** axes are the tangential, axial, and radial direction, respectively, as illustrated in Figure 3, and l_f and l_s are radial length of the fluid and adjacent solid element, respectively, as shown in Figure 4.

Previous literature studied the former topic and demonstrated that the largest mesh size along **v** axis should be smaller than one-twelfth of the water depth [20], but little literature has been found on the latter. Therefore, we take the fully immersed experimental case ($H_r = 0.55$ m) as the reference and build the pile-water interaction FE model using 3D PBFEs. As shown in Figure 3, the testing pile and the surrounding water domain are discretized into 8-node solid and 8-node potential-based finite elements, respectively. Fluid-structure interface elements (Figure 1(a)) are used to connect the PBFEs with the adjacent solid elements. Free surface interface elements (Figure 1(b)) are placed onto the top boundary of the PBFE volume to prescribe the zero pressure and displacement of the top bounding surface. The other bounds of fluid domain are covered with rigid-wall interface elements (Figure 1(d)) to consider the disallowance condition on the basin wall.

The effects of mesh size along direction **w** are then investigated through parametrical analyses of the ratio l_f/l_s. The solid domain along **u**, **v**, and **w** axes is evenly divided into 20, 12, and 4; hence, $l_s = 0.0146/4 = 3.65e-3$. The fluid domains along **u** and **v** axes are evenly 20 and 12. Those

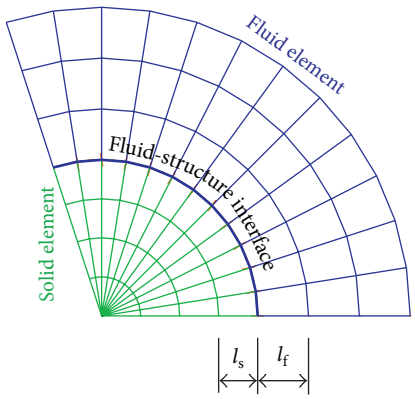

Figure 4: Discretization of elements beside the fluid-structure interface.

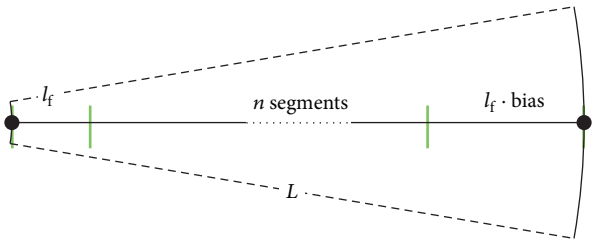

Figure 5: Subdivision of the **w** edge of the water domain.

divisions are unchanged during the whole study, while the fluid division along **w** is the only variable.

Here we use the geometric subdivision instead of average subdivision to divide the fluid domain bound line along **w** axis. Geometric subdivision is more general and allows user to use the subdivision number n and the ratio bias ((n–1)th power of the common ratio) and to control the innermost element size l_f together. Figure 5 shows the geometric subdivision example, where L is the total length of the water domain. The relationship between l_f and bias and n is denoted by the following:

$$l_f = L\frac{1 - \text{bias}^{1/(n-1)}}{1 - \text{bias}^{n/(n-1)}}. \tag{19}$$

When bias equals 1, we can calculate the limit from (19) that $l_f = L/n$, which turns a geometric into an average subdivision. The mesh size l_f decreases only with the increase of the division number n. An increase of n from 10 to 1000 leads to a decrease of the ratio l_f/l_s from 26 to 0.7. Figure 6 shows the fundamental frequency for the pile as a function of l_f/l_s and n for bias = 1. In order to illustrate this clearly, the values of l_f/l_s are originally drawn on x axis by log2 scale.

When the meshing divisions n are a constant of 15, an increase of bias will also lead to the decrease of l_f/l_s according to (19). The fundamental frequency for the pile as a function of l_f/l_s and bias for n = 15 is shown in Figure 7.

An interesting conclusion is drawn from Figures 6 and 7 that no matter which division progression is used, once the ratio l_f/l_s along **w** axis approaches to 1, the result of the frequency analysis converges. But compared with the former

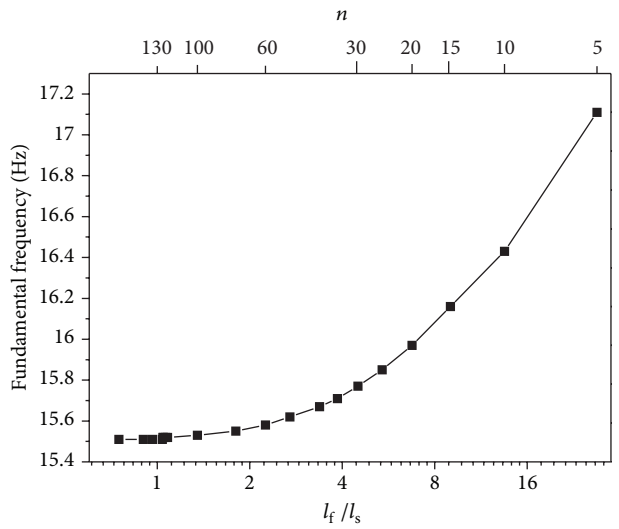

Figure 6: The fundamental frequency for the pile as a function of l_f/l_s and n, for bias = 1.

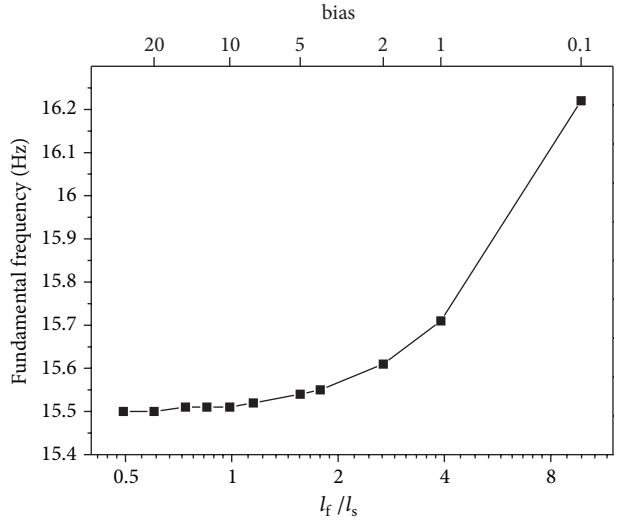

Figure 7: The fundamental frequency for the pile as a function of l_f/l_s and bias, for n = 15.

equally division, the latter requires less girds and is more economic. According to the finding, we set the number of meshing subdivisions for pile in directions **u**, **v**, and **w** to 20, 12, and 4, respectively, and for water to 20, 12, and 50, respectively. The **w**-axis bias of water domain equals 5, which gives $l_s = 3.88e-3$ and makes the ratio l_f/l_s approach to 1. The FE frequency analyses using the refined numerical models are carried out for water levels of 0, 0.44 m, 0.52 m, and 0.55 m, respectively.

3.3. Exact Analytical Solution. For the experimental pile shown in Figure 2, the equation of motion of the pile subjected to ground motion $\ddot{u}_g(t)$ along the first mode

of vibration can be obtained as the analytical approach developed by Liaw and Chopra [13]:

$$M_1\ddot{Y}_1(t) + 2\xi_1\omega_1 M_1\dot{Y}_1(t) + \omega_1^2 M_1 Y_1(t) = -M_1'\ddot{u}_g(t) - F_1(t), \tag{20}$$

where Y_1 is the corresponding generalized coordinate, ξ_1 is the structural damping ratio, and ω_1 is the vibration frequency along the first modal shape of vibration ψ_1 of the pile without water. For a cantilever beam with a free end [14],

$$\omega_1 = (1.875)^2\sqrt{\frac{EI}{\mu_s H_s^4}}, \tag{21}$$

$$\psi_1 = \cos\left(\frac{1.875}{H_s}x\right) - \cosh\left(\frac{1.875}{H_s}x\right) - 0.734\left[\sin\left(\frac{1.875}{H_s}x\right) - \sinh\left(\frac{1.875}{H_s}x\right)\right]. \tag{22}$$

The parameters M_1, M_1', and F_1 are given by

$$M_1 = \int_0^{H_s}\mu_s\psi_1(z)^2\,dz, \tag{23a}$$

$$M_1' = \int_0^{H_s}\mu_s\psi_1(z)\,dz, \tag{23b}$$

$$F_1(t) = \int_0^{H_s}\int_0^{2\pi} p_s(z,\theta,t)\,r_s\cos(\theta)\,\psi_1(z)\,d\theta\,dz, \tag{23c}$$

in which $p_s(\theta, z, t)$ denotes the hydrodynamic pressure applied at the outer lateral surface of the cylinder pile and r_s is the radius of the pile. Considering a harmonic ground acceleration $\ddot{u}_g(t) = e^{i\omega t}$, the radial hydrodynamic pressure p_s, the generalized coordinate $Y_1(t)$, and its double time derivative $\ddot{Y}_1(t)$ can be obtained as

$$p_s(z,\theta,t) = \overline{p}_s(z,\theta,\omega)\,e^{i\omega t}, \qquad Y_1(t) = \overline{Y}_1(\omega)\,e^{i\omega t},$$
$$\ddot{Y}_1(t) = \overline{\ddot{Y}}_1(\omega)\,e^{i\omega t} = -\omega^2\,\overline{Y}_1(\omega)\,e^{i\omega t}. \tag{24}$$

The frequency response function $\overline{p}_s$ for hydrodynamic pressure can be decomposed as

$$\overline{p}_s(z,\theta,\omega) = \overline{p}_0(z,\theta,\omega) + \overline{\ddot{Y}}_1(\omega)\,\overline{p}_1(z,\theta,\omega), \tag{25}$$

in which $\overline{p}_0$ is the hydrodynamic pressure frequency response functions corresponding to a rigid body motion of the cylinder pile $\psi_0 = 1$ and $\overline{p}_1$ is the hydrodynamic pressure corresponding to the first modal shape for the cantilever beam with a free end ψ_1 given by (22). Using (20) and (25), the frequency response function $\overline{\ddot{Y}}_1(\omega)$ can be expressed as

$$\overline{\ddot{Y}}_1(\omega) = \frac{M_1' + B_0(\omega)}{M_1\left[-1 + 2i\xi_1(\omega_1/\omega) + (\omega_1/\omega)\right] - B_1(\omega)}, \tag{26}$$

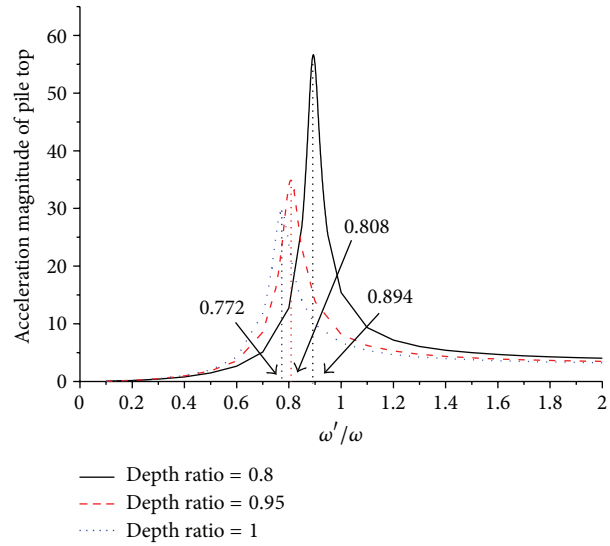

Figure 8: Analytical frequency response curves of the structural acceleration at mid-point of the pile.

Table 1: Fundamental frequency (in Hz) of cylinder pile tested in water with different levels (in m).

Water level H_r	H_r/H_s	PBFE	Experiment (Zhang, [23])	Analytical
0	0	21.02	20.75	20.79
0.44	0.8	18.21	18.30	18.59
0.52	0.95	16.28	17.09	16.79
0.55	1	15.50	15.90	16.04

where

$$B_k(\omega) = \int_0^{H}\int_0^{2\pi}\overline{p}_k(\theta,z,\omega)\,r_s\cos(\theta)\,\psi_1(z)\,d\theta\,dz, \quad k = 0, 1. \tag{27}$$

The equations governing the hydrodynamic pressures $\overline{p}_0$ and $\overline{p}_1$ and the corresponding boundary conditions were given by Liaw and Chopra. Details of the frequency-dependent solutions for $\overline{p}_k$ can be found in the literature [13] and are not reproduced here for brevity.

The fundamental frequency of the pile-water system is obtained using a harmonic sweep frequency response analysis [14]. Programme the analytical formulations and solve (26) in time domain with an array of forcing frequencies covering the range 0 to $2\omega_1$. An acceleration frequency response is then determined and the fundamental natural frequency ω_1' of the immersed pile is obtained as the frequency ratio ω'/ω_1 corresponding to the resonant peak. The acceleration magnitude value of frequency response curves for the experimental pile submerged in different water levels is given in Figure 8.

3.4. Comparison of the Results. The fundamental natural vibration frequencies obtained are presented in Table 1 for the PBFE numerical, exact analytical, and experimental results,

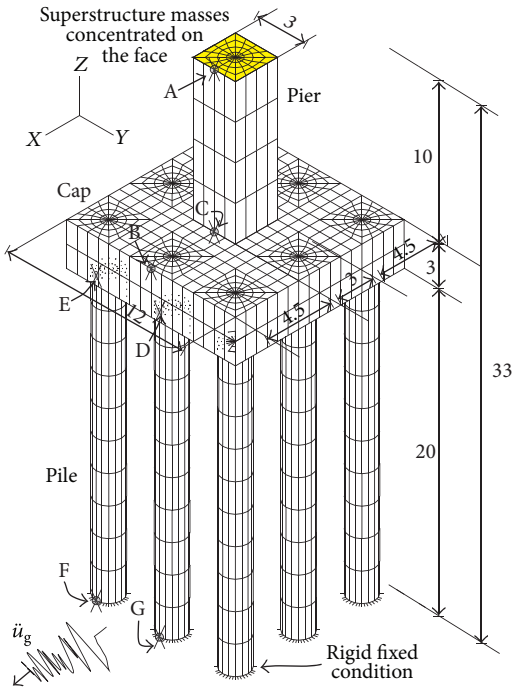

FIGURE 9: Geometry and meshing details of the pile foundation (unit: m).

respectively, as a function of water depth ratios H_r/H_s varying from 0 to 1 for the empty to the full reservoir, respectively. It shows that the PBFE results agree well with the experimental and the analytical curves. The PBFE has very good efficiency and accuracy in 3D frequency analysis of pile-water system.

4. Seismic Response of a Deep Water 9-Pile Foundation

4.1. Modeling and Analysis. A concrete piled foundation of a continuous bridge crossing Songhua River, China, is taken as the background. The material of the foundation is C30 concrete [11]. The bridge superstructure, such as girders and bearings, are simplified into a 3×10^6 kg concentrated mass on top of the pier and the pile-soil interaction is neglected since present work mainly focuses on investigating the effect of fluid-structure interaction between the foundation and water. The 3D finite element model for the foundation structure is depicted in Figure 9. The fundamental period of vibration T_1 of the 9-pile foundation structure is 1.103 s.

In order to investigate the effect of surrounding water on the seismic response of a pile-group foundation, the PBFE techniques validated above are then used to carry out the time-history analyses of the pile group foundation at dry (water depth $H_r = 0$ m), half-wet (water depth $H_r = 12$ m), and wet (water depth $H_r = 23$ m) conditions, respectively. For the wet case, all the cap and the piles are immersed, while for the half-wet case, only the lower part of the piles is immersed.

For illustration purpose, Figure 10 shows the geometry and x-, y-cutting planes of the PBFEs model used for the wet case. The water domain has a length of 52 m, a width of 36 m, and a height of 23 m. Based on the validated approach, a total of 4512 8-node solid elements and 19360 8-node PBFEs are produced in the fluid-structure coupled finite element model. The following material properties are considered: a modulus of elasticity $E_c = 32500$ MPa, a Poisson's ratio $\nu = 0.2$, and a density $\rho_s = 2500$ kg/m^3 for concrete and a velocity of pressure waves of $C_r = 1440$ m/s, a density $\rho_w = 1000$ kg/m^3, and a bulk modulus $\mu_r = 2.3 \times 10^3$ MPa for water. The Rayleigh damping matrix is used with a ratio of 0.05 at control frequency. The free surface, fluid-structure, and infinite interface elements are applied to specify the related boundary conditions.

The submerged pile foundation is subjected to the unscaled S-N component of the 1994 Northridge-02 earthquake record at Hollywood (NGA1660) along the x-axis direction. The record is downloaded from PEER NGA strong motion database [24], which is shown in Figure 11 with a peak ground acceleration of 0.159 g and a preferred Vs30 of 316.50 m/s. Linear time-history analyses of the three cases are then carried out to obtain the following responses: x-displacements of points A (the top of the pier) and B (the top of pile-cap) and the maximum effective stress of points C (the bottom of pier), D (the top of the middle pile), E (the top of the side pile), F (the bottom of the side pile), and G (the bottom of the middle pile). The location of these points is detailed in Figure 9.

5. Discussion

Table 2 presents the seismic responses of dry, half-wet, and wet case. It is clearly seen from the comparison between results of case considering water and that of dry case that the earthquake-induced fluid-structure interaction alters the structural seismic response. When the cap and piles are all immersed, the earthquake-induced fluid-structure interaction increases the displacement at the top of the pier (point A) but decreases the displacement of the cap (point B) slightly. The existing of surrounding water increases the force of the pile, especially the bottom force of pile (points F and G) but reduces nearly 18% of the bottom force of the pier (point C). Figure 12 compares the dry and wet time histories of the effective stress at point C. The hydrodynamic effect alters the response amplitude without changing the phase clearly. And the hydrodynamic effects influence the middle pile (points D and G) greater than the side pile (points E and F). The difference may be caused by the pile-group effect. The seismic force of the piles should be paid more attention during the seismic design of deep water pile foundation.

Some interesting conclusions also can be drawn from the comparison of the results as a function of water depths varying from 0 to 23 m. The earthquake-induced fluid-structure interaction increased with the water depth. Compared with the responses of half-wet case, the fully immersed cap of wet case significantly increases the fluid-structure interactions and their influences. The influence of the water-pile interaction on the seismic response is too weaker to be ignored, compared to that of the cap-water interaction. Hence, the fluid-structure interaction is strongly recommended to be

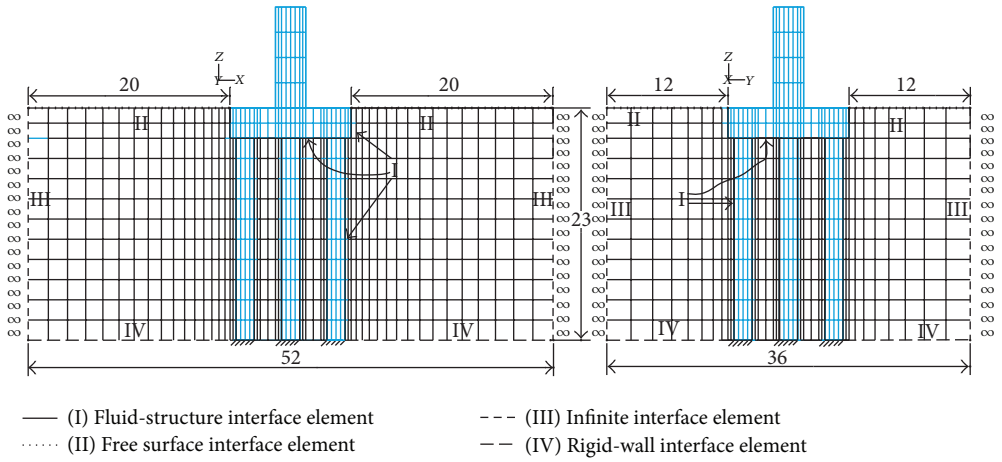

Figure 10: Geometry and x-, y-cutting planes of the PBFE model (unit: m).

Table 2: Absolute maximum envelops of principle structural stress and displacement due to seismic loads.

Point	A	B	C	D	E	F	G
Response	X Disp, m	X Disp, m	Effective Stress, MPa	Effective Stress, MPa	Effective Stress, MPa	Effective Stress, MPa	Effective Stress, MPa
0 m (Dry)	$4.85E-03$	$3.85E-03$	0.58	0.59	0.633	0.893	0.901
12 m (Half-wet)	$4.86E-03$	$3.84E-03$	0.56	0.59	0.633	0.902	0.912
23 m (Wet)	$4.91E-03$	$3.79E-03$	0.47	0.603	0.635	0.938	0.952
Error $\frac{(\text{Half-Wet}-\text{Dry})}{\text{Dry}}$	0.21%	−0.25%	−3.45%	0.67%	0.06%	1.00%	1.22%
Error $\frac{(\text{Wet}-\text{Dry})}{\text{Dry}}$	1.38%	−1.56%	−18.91%	2.08%	0.31%	5.00%	5.73%

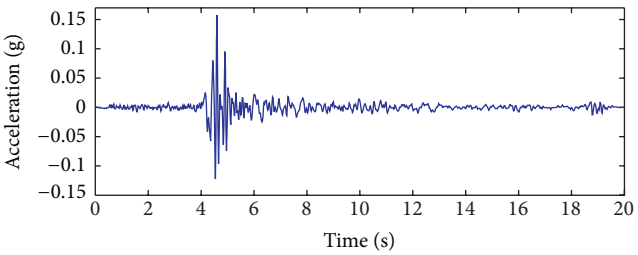

Figure 11: Time history of Northridge earthquake at Hollywood.

considered for a bridge with its cap of foundation submerged in the water.

The successful analyses state that the potential-based fluid elements and the interface elements discussed previously perform well for seismic analyses of pile foundation-water systems. The earthquake-induced fluid-structure interaction effect on the response of the structure is a very complex effect. It is difficult to draw general conclusions from the phenomenons whether the hydrodynamic effect due to seismic ground motion is beneficial or detrimental to the structural response as a whole, but we can draw some good advices from this investigation.

6. Conclusions

In this paper, we derived the formulation of the potential-based fluid formulation mathematically and presented the mechanism of interface elements for reference. We took an experimental case ($H_r = 0.55$ m) as the reference and built the pile-water interaction FE model using 3D PBFEs. The key subdivision problem of PBFE modeling was investigated through parametrical analyses. The PBFE approach was then validated experimentally and analytically. Finally, a case study of the seismic analysis for a typical bridge pile-group foundation is then carried out based on the validated approach. The main findings of this study are the following.

(1) The potential-based fluid elements approach performs adequately for 3D frequency- and time-domain seismic analyses of pile foundation-water systems and can be an alternative method for future study.

(2) During the fluid-structure interaction modeling using PBFEs, once the size ratio of the adjacent solid

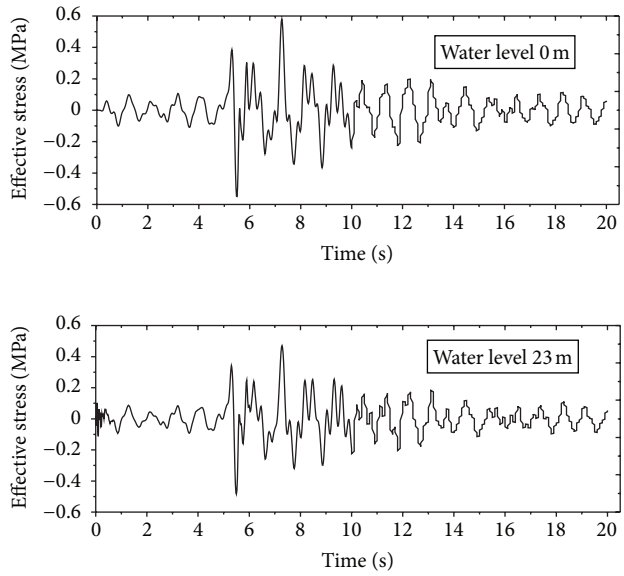

FIGURE 12: Time history of effective stress at point C for $H_r = 0$ m and 23 m.

and fluid element along **w**-axis approaches 1, the analysis converges.

(3) The fluid-structure interaction is strongly recommended to be considered for a bridge with its cap of foundation submerged in the water. The seismic force of the piles should be paid more attention during the design.

Conflict of Interests

The authors would like to clearly state that they did not have any financial relations with any commercial entities and did not mean the research to be influenced by any financial interests. The references of the commercial numerical analyses tool have been removed to eliminate any conflict of interests regarding the submission and publication of the paper and its potential implications.

Acknowledgments

This research is supported by the National Science Foundation of China (Grant no. 51278376 and 90915011) and Kuang-Hua Fund for Civil Engineering College, Tongji University. The authors would like to acknowledge their support gratefully.

References

[1] M. Feng, "China's Major Bridges," in *Proceedings of the International Association for Bridge and Structural Engineering Symposium (IABSE '09)*, pp. 1–24, Shanghai, China, 2009.

[2] T. J. Ingham, S. Rodriguez, R. Donikian, and J. Chan, "Seismic analysis of bridges with pile foundations," *Computers and Structures*, vol. 72, no. 1, pp. 49–62, 1999.

[3] S. S. Abdelsalam, S. Sritharan, and M. T. Suleiman, "Current design and construction practices of bridge pile foundations with emphasis on implementation of LRFD," *Journal of Bridge Engineering*, vol. 15, no. 6, pp. 749–758, 2010.

[4] Q. You, X. Zhang, L. Feng, and H. Liu, "Sutong Bridge—a thousand-meter span cable-stayed bridge across Yangtze River," in *Proceedings of the 24th Annual International Bridge Conference*, Pittsburgh, Pa, USA, 2007.

[5] C. Lin, C. Bennett, J. Han, and R. L. Parsons, "Integrated analysis of the performance of pile-supported bridges under scoured conditions," *Engineering Structures*, vol. 36, pp. 27–38, 2012.

[6] M. R. Maheri and R. T. Severn, "Experimental added-mass in modal vibration of cylindrical structures," *Engineering Structures*, vol. 14, no. 3, pp. 163–175, 1992.

[7] A. Uściłowska and J. A. Kołodziej, "Free vibration of immersed column carrying a tip mass," *Journal of Sound and Vibration*, vol. 216, no. 1, pp. 147–157, 1998.

[8] H. R. Öz, "Natural frequencies of an immersed beam carrying a tip mass with rotatory inertia," *Journal of Sound and Vibration*, vol. 266, no. 5, pp. 1099–1108, 2003.

[9] J. R. Morison, M. P. O. 'Brien, J. W. Johnson, and S. A. Schaaf, "The force exerted by surface waves on piles," *AIME Petroleum Transactions*, vol. 189, pp. 149–154, 1950.

[10] R. E. Taylor, "A review of hydrodynamic load analysis for submerged structures excited by earthquakes," *Engineering Structures*, vol. 3, no. 3, pp. 131–139, 1981.

[11] Ministry of Communications of China, "Guidelines for seismic design of highway bridges," JTG/T B02-01-2008, Beijing, China, 2008.

[12] M. S. Park, W. Koo, and K. Kawano, "Dynamic response analysis of an offshore platform due to seismic motions," *Engineering Structures*, vol. 33, no. 5, pp. 1607–1616, 2011.

[13] C. Y. Liaw and A. K. Chopra, "Dynamics of towers surrounded by water," *Earthquake Engineering and Structural Dynamics*, vol. 3, no. 1, pp. 33–49, 1974.

[14] K. Wei, W. C. Yuan, N. Bouaanani, and C. C. Chang, "An improved HSFR method for natural vibration analysis of an immersed cylinder pile with a tip mass," *Theoretical and Applied Mechanics Letters*, vol. 2, no. 2, Article ID 023002, 4 pages, 2012.

[15] J. S. Wu and C. T. Chen, "An exact solution for the natural frequencies and mode shapes of an immersed elastically restrained wedge beam carrying an eccentric tip mass with mass moment of inertia," *Journal of Sound and Vibration*, vol. 286, no. 3, pp. 549–568, 2005.

[16] J. T. Xing, W. G. Price, and Y. G. Chen, "A mixed finite-element finite-difference method for nonlinear fluid-structure interaction dynamics. I. Fluid-rigid structure interaction," *Proceedings of the Royal Society A*, vol. 459, no. 2038, pp. 2399–2430, 2003.

[17] N. Bouaanani and B. Miquel, "A new formulation and error analysis for vibrating dam-reservoir systems with upstream transmitting boundary conditions," *Journal of Sound and Vibration*, vol. 329, no. 10, pp. 1924–1953, 2010.

[18] G. C. Everstine, "A symmetric potential formulation for fluid-structure interaction," *Journal of Sound and Vibration*, vol. 79, no. 1, pp. 157–160, 1981.

[19] K. J. Bathe, H. Zhang, and S. Ji, "Finite element analysis of fluid flows fully coupled with structural interactions," *Computers and Structures*, vol. 72, no. 1–3, pp. 1–16, 1999.

[20] N. Bouaanani and F. Y. Lu, "Assessment of potential-based fluid finite elements for seismic analysis of dam-reservoir systems," *Computers and Structures*, vol. 87, no. 3-4, pp. 206–224, 2009.

[21] L. G. Olson and K. J. Bathe, "A study of displacement-based fluid finite elements for calculating frequencies of fluid and fluid-structure systems," *Nuclear Engineering and Design*, vol. 76, no. 2, pp. 137–151, 1983.

[22] L. G. Olson and K. J. Bathe, "An infinite element for analysis of transient fluid-structure interactions," *Engineering Computations*, vol. 2, no. 4, pp. 319–329, 1985.

[23] M. Zhang, *Vibration analysis of solid-fluid interaction for the Pier-river water [M.S. thesis]*, Dalian Jiaotong University, 1993.

[24] Pacific Earthquake Engineering Research Center (PEER), "NGA Database," 2013, http://peer.berkeley.edu/nga/data?doi=NGA1660.